# NUMERICAL INVESTIGATION OF TURBULENT FLOW AND HEAT TRANSFER OVER PARTIALLY OPEN CAVITIES
## Effect of Opening Ratio

by

***Mohamed M. ABO ELAZM*, Ali I. SHEHATA, and Khalid M. SAQR***
Mechanical Engineering Department, College of Engineering and Technology,
Arab Academy for Science, Technology and Maritime Transport,
Abu Qir, Alexandria, Egypt

Original scientific paper
https://doi.org/10.2298/TSCI150309126A

*Partially open cavities are encountered in various engineering systems such as electronic cooling devices and cooling for gas turbine blades, instead of conventional film cooling slots. Flow is to be imparted over the partially open cavity where it induces a shear layer and a shear driven vortex within the cavity, which is subjected to cooling effect at its wall. Depending on the opening ratio, heat and mass transfer occur between the main flow and the trapped vortex through the shear layer. In the present study, RANS simulations of such flow have been conducted for circular and square cavities to investigate the effect of opening ratio on the heat and mass transfer characteristics. The simulations were established on a rigorous numerical approach and proper validation with laser Doppler velocimetry measurements of turbulent flow in circular cavity. Based on the hydraulic diameter of the cavity, opening ratios ranging from 0.2 to 1.0 were investigated for a Reynolds number of $3 \cdot 10^5$. Generally, the maximum Nusselt number was achieved at higher opening ratios for both circular and rectangle cavities. On the other hand, the maximum dimensionless temperature gradient, $\theta$, inside the cavity was achieved at L/D = 0.2 for both cavity configurations.*

Key words: *partially open cavity, turbulent flow, RANS, heat transfer, opening ratio*

## Introduction

The problem of shear/lid driven cavity flow has an important relevance to numerous engineering applications such as heat exchangers [1, 2], flight aerodynamics [3, 4] and combustion and turbomachinery [5, 6]. In addition, the problem has a long history as a fundamental fluid mechanics benchmark case for the development of numerical codes for the solution of Navier-Stokes equation [7]. In this paper, cavity flow is utilized to provide a cooling mechanism for turbine blades, as a replacement for the traditional cooling slots. There are several disadvantages associated with the conventional methods of film cooling including energy loss [8] as well as increased levels of entropy generation due to impingement action and its associated vortex structure [9, 10]. There have been numerous attempts to improve the performance of film cooling [11-14], however, the former disadvantages could not be avoided. In the present work, a partially open cavity is used to replace the cooling slot. When the flow passes this cavity, it

* Corresponding author, e-mail: maboelazm@gmail.com; m.aboelazm@aast.edu

creates a shear driven flow inside the cavity, which allows efficient forced convection to take place. The entrainment of the flow within the shear layer creates a film cooling effect, similar to such created by the jet impingement, however, without sacrificing the heat energy loss in the system. A schematic of the partially open cavity is shown in fig. 1. When the hot gasses entrain to the cavity, the temperature decreases inside the cavity and the recirculated gases cools down the surface downstream the cavity.

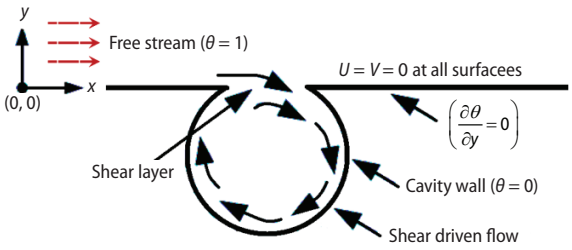


**Figure 1. The flow configuration of the partially-open cavity**

Although literature records cite very few references discussing forced convection and turbulent flow over partially open cavities, natural convection in partially open cavities has been investigated in a number of studies. Unlike the latter studies which focus on the flow physics, most of the former references adopted the turbulent flow over partially open cavity as a validation case for numerical approaches. Syed and Hoffmann [15] conducted detached eddy simulation for turbulent flow over a partially open cavity. Their work has mainly aimed at comparing three sub-grid scale turbulence models, namely the S-A, SST $k$-$\omega$, and the realizable $k$-$\varepsilon$ models. Saqr *et al.* [16] have conducted CFD investigation of turbulent flow over a partially-open circular cavity using the $R_\varepsilon/k$-$\varepsilon$ turbulence model. The main objective of their work was to test the additional source term in the $\varepsilon$ equation, which represents local anisotropy. Xia and Zhou [17] investigated the natural convection in an externally heated partially open cavity. They have used a numerical approach to compute the heat transfer characteristics within the cavity at different Rayleigh numbers and opening ratios. They found that the opening ratio affects the thermally driven flow within the cavity as well as the heat transfer characteristics. Bilgen and Oztop [18] have conducted numerical investigation of laminar natural convection in inclined partially open cavities. They found that the Nusselt number and flow structure are directly related to the opening size and Rayleigh number.

On the other hand film cooling technique has been studied experimentally and numerically. Azzi and Jubran [19] introduced a converging slot hole designed as a film cooling improvement concept. Direct numerical simulation was executed and compared to the standard cylindrical cooling tube as well as a shaped cylindrical layout. The slot increased the film cooling effectiveness, also the span coverage of the coolant jet when compared to the other two layouts for the same blowing ratio. Bogard and Thole [20] mentioned that the manufacturing of shaped film cooling holes is a highly significant parameter in blade design, since the difference in cost between manufacturing simple cylindrical holes and shaped is high.

Liu *et al.* [21] executed an experimental study using liquid crystal thermography, comparing converging slots holes to standard cylindrical holes at a range of momentum flux ratios. The coolant jet of the slots was much more attached to the surface of the blade and as a result a much higher film cooling effectiveness has been achieved when compared to the standard cylindrical holes and shaped holes with different compound angles. The shaped hole with a 45º compound angle improved the film cooling effectiveness by 150% to 200% in some areas when compared with the baseline geometry. Haven [22] concluded in her experimental study on film cooling sensitivity to the hole shape, that the jet liftoff and hot gas entrainment toward the surface is highly affected by the proximity of the counter rotating vortex pair (CRVP) relative to one another. It was shown that large aspect ratio geometries tend to liftoff less than their smaller coun-

terparts. An experimental study has been executed by Baldauf *et al.* [23] comparing film cooling effectiveness for several blowing ratios under engine like conditions, it was shown that for blowing ratios from 0.2 to 0.85 the film cooling effectiveness increases with the increase of the blowing ratio, the top film cooling effectiveness is for a blowing ratio between 0.85 and 1.2, beyond this region the film cooling effectiveness starts decreasing with the blowing ratio increase.

Thole *et al.* [24] studied the effect of the momentum flux ratio $I$ and the jet behavior. It was shown that there are three main jet behaviors with the mainstream. For $I < 0.4$ the jet is fully attached to the blade surface, and for $I > 0.8$ the jet is fully detached from the surface. As for the $0.4 < I < 0.8$ the jet detach and reattach soon to the blade surface. Kadotani and Goldstein [25] performed various studies on the effect of mainstream variable on film cooling and it was shown that a thin mainstream boundary-layer would give higher film cooling effectiveness when compared with large boundary-layer thickness, due to the stronger momentum of the thin boundary-layer impacting the jet. It thus, improves the jet attachment to the surface. Leylek and Zerkle [26] executed the first numerical simulation of a 3-D film cooling jet in cross-flow problem using the standard $k$-$\varepsilon$ turbulence model with wall function. The authors slightly over predicted the center line film cooling effectiveness for a fully attached jet. While, Ferguson *et al.* [27] showed that it is more difficult to predict the film cooling effectiveness for detached jets using a variety of different turbulence models versions, with both wall function, and a two layer wall treatment algorithm. Lakehal *et al.* [28] adopted a wall function to model lateral injection film cooling, using the standard $k$-$\varepsilon$ model. The model predicted CRVP and the jet trajectory, as well as the temperature gradient between the core of the jet and the mainstream, but could not well predict the lateral spreading of the coolant.

The literature review has mainly revealed two features of the present topic. The first is the scarcity of studies discussing turbulent flow and forced convection over partially open cavities. The second feature highlighted the challenges facing the state of the art film cooling technology. The scope of the present work links those two features by studying the concept of film cooling via partially open cavities.

Considering the various possibilities of such cavities in terms of geometry and opening ratio, the objectives of the present work aimed at characterizing and comparing the flow and heat transfer over square and circular cavities with different opening ratios. The major objective was to investigate the effect of geometry and opening ratio on the heat transfer characteristics downstream the cavity. The secondary objectives aimed to analyze the effect of cavity shape and opening ratio on the flow structure and heat transfer within the cavity.

## Configurations of the flow over partially open cavities

Assuming 3-D symmetry, 2-D open cavities with circular and square cross-sections were considered for the present study as shown in fig. 2(a). The hot surface was segmented and simplified to a flat horizontal plate. The opening ratio, $L/D$, for both circular and square cavities is variable in the range of ($L/D$ = 0.2, 0.4, 0.6, 0.8, and 1.0). The flow is numerically imparted via Drichlet boundary condition from the left side at ($\mathrm{Re} = 3 \cdot 10^5$) and (2%) turbulence intensity. Where Reynolds number was calculated based on the reference velocity, $U_{\mathrm{ref}}$. The inlet velocity was set to a constant x-component with a uniform distribution along y-axis, and a logarithmic distribution according to the law-of-the-wall, as shown in section *Computational approach*. The boundary condition at the exit plane of the domain was set to a constant pressure type, with a value corresponding to atmospheric conditions. The upper boundary of the domain was assigned a slip boundary condition to eliminate the wall effect.

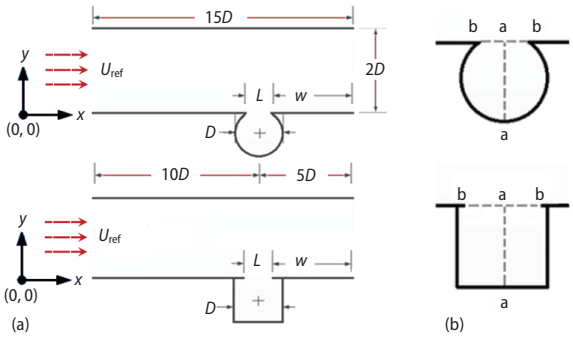


**Figure 2. Schematics of (a) 2-D computational domain showing characteristic dimensions as function of the cavity hydraulic diameter, *D*, and (b) section (a-a) and (b-b) within the cavity region**

The Prandtl number was fixed at 0.71, which allowed the analysis of the dominant forced convection regime. The entrance and exit of the main stream is fixed at $2D$, while the hydraulic diameter is defined as $D$. No slip boundary condition was set for all walls except the upper wall was set to slip velocity condition. Regarding thermal boundary conditions, adiabatic walls were assumed except the cavity wall where the heat transfer takes place. The non-dimensional temperature of the inlet hot flow is fixed at $\theta = 0$ while the isothermal cold cavity wall is fixed at $\theta = 1$, where $\theta$ is defined:

$$\theta = \frac{T_h - T}{T_h - T_c} \tag{1}$$

## Mathematical model and computational approach

### *Governing equations*

The governing equations of the present turbulent non-isothermal flow are steady incompressible continuity and the RANS equations:

– continuity

$$\frac{\partial}{\partial x_i}\left[\overline{u}_i\right] = 0 \tag{2}$$

– RANS

$$\frac{\partial}{\partial x_i}\left(\rho\overline{u}_i\overline{u}_j\right) = -\frac{\partial p}{\partial x_i} + \frac{\partial}{\partial x_j}\left[\mu\left(\frac{\partial \overline{u}_i}{\partial x_j} + \frac{\partial \overline{u}_j}{\partial x_i} - \frac{2}{3}\delta_{ij}\frac{\partial \overline{u}_j}{\partial x_i}\right)\right] + \frac{\partial}{\partial x_j}\left(-\overline{\rho u_i' u_j'}\right) \tag{3}$$

#### *Turbulence modeling*

Boussinesq turbulent viscosity assumption [29] was used to close the Reynolds stress term in eq. (3), so that:

$$-\overline{\rho u_i' u_j'} = \mu_t\left(\frac{\partial \overline{u}_i}{\partial x_j} + \frac{\partial \overline{u}_j}{\partial x_i}\right) - \frac{2}{3}\rho k\delta_{ij}$$

The turbulent viscosity, $\mu_t$, was modeled using two turbulence models for the validation case; namely the $k$-$\varepsilon$ [30, 31] and the $\overline{v^2}$-$f$ [32] turbulence models. The standard $k$-$\varepsilon$ model equations are given:

– turbulence kinetic energy equation

$$\rho\frac{\partial}{\partial x_i}\left[U_i k\right] = \frac{\partial}{\partial x_j}\left[\left(\mu + \frac{\mu_T}{\sigma_k}\right)\frac{\partial}{\partial x_j}k\right] + \mu_T S^2 - \rho\varepsilon \tag{4}$$

– dissipation rate equation

$$\rho\frac{\partial}{\partial x_i}\left[U_i\varepsilon\right]=\frac{\partial}{\partial x_j}\left[\left(\mu+\frac{\mu_T}{\sigma_\varepsilon}\right)\frac{\partial}{\partial x_j}\varepsilon\right]+C_{\varepsilon 1}\frac{\varepsilon}{k}\mu_T S^2-C_{\varepsilon 2}\rho\frac{\varepsilon^2}{k} \tag{5}$$

– turbulent viscosity

$$\mu_T=\rho C_\mu\frac{k^2}{\varepsilon} \tag{6}$$

where $C_{\varepsilon_1}$=1.44, $C_{\varepsilon_2}$=1.92, $C_\mu$ = 0.09, $\sigma_k$ = 1.0, and $\sigma_\varepsilon$ =1.3

In addition to eqs. (4) and (5), the $\overline{v^2}$-$f$ model solves two equations for the velocity scale $\overline{v^2}$ and elliptic relaxation function $f$ [32]. The transport equations for these variables can be given:

– velocity scale

$$\rho U_j\frac{\partial\overline{v^2}}{\partial x_j}=kf-\frac{\overline{v^2}}{k}\varepsilon+\frac{\partial}{\partial x_j}\left[\left(\mu+\frac{\mu_T}{\sigma_{\overline{v^2}}}\right)\frac{\partial\overline{v^2}}{\partial x_j}\right] \tag{7}$$

– elliptic equation for the relaxation function

$$L^2\nabla^2 f-f=\frac{C_1-1}{T}\left(\frac{\overline{v^2}}{k}-\frac{2}{3}\right)-C_2\frac{\mu_t S^2}{\varepsilon} \tag{8}$$

where the turbulence length scale, $L$,

$$L=C_L\max\left(\frac{\sqrt{k^3}}{\varepsilon},C_\eta\sqrt[4]{\frac{\nu^3}{\varepsilon}}\right) \tag{9}$$

the turbulence time scale, $T$,

$$T=\max\left(\frac{k}{\varepsilon},C_T\sqrt{\frac{\nu}{\varepsilon}}\right) \tag{10}$$

and the turbulent viscosity is calculated from

$$\mu_T^{\overline{v^2}}=\rho^{\overline{v^2}}C_\mu\overline{v^2}T \tag{11}$$

where the model coefficients are given as: $C_\mu=0.22$, $\sigma_{\overline{v^2}}=1$, $C_1$ = 1.4, $C_2$ = 0.45, $C_T=6$, $C_L=0.25$, and $C_\eta=85$.

### *Computational approach*

The general purpose CFD package FLUENT 6.3 was used to conduct the analysis [33]. The steady pressure based solver was used with the SIMPLE algorithm, where the momentum, continuity, and energy equations are solved consecutively and the turbulence closure is used to correct the velocity field during iterations. Second order discretization scheme was used with all terms of the governing equations. The space was discretized using structured

cells, which were subjected to a size function to enable small cells to be located in the near wall region. This is done to resolve the boundary-layer with sufficient accuracy. The computational grids for circular and square cavities are shown in fig. 3. For the *k-ε* model, the logarithmic law of the wall was used to predict the near-wall velocity as proposed in [34]. Such law expresses the mean near-wall velocity:

$$U^* = \frac{1}{k}\ln\left(Ey^*\right) \tag{12}$$

and

$$y^* \equiv \frac{1}{\mu}\rho\sqrt[4]{C_\mu}\sqrt{k_p}y_p \tag{13}$$

where $k = 0.4187$ is von Karman constant, $E = 9.793$ – the empirical constant, $k_p$ – the turbulence kinetic energy at point $p$, and $y_p$ – the distance between point $p$ and the wall. The law in eq. (12) is valid for $30 < y^* < 300$. In all the simulation cases presented here, $y^*$ was maintained in the range of (50 to 90) to ensure the applicability of the Log law of the wall.

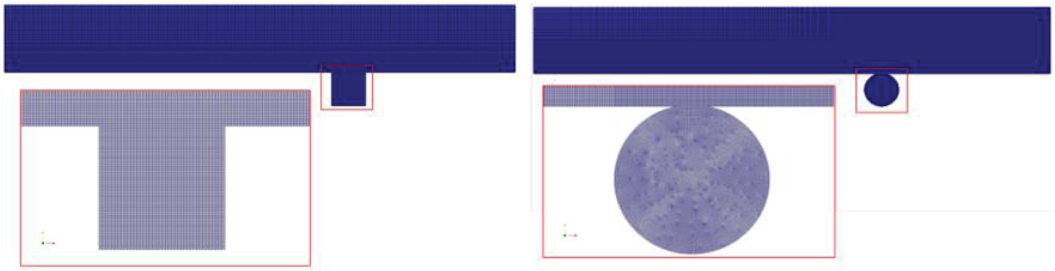


**Figure 3. Computational domain for (a) square cavity and (b) circular cavity**

The cell sizing was done based on a grid sensitivity analysis, which showed that grids with more than $8.9 \cdot 10^4$ produce grid-independent solutions. The settings and the results of the grid sensitivity analysis for cases (C-0.6 and S-0.6) are presented in tab. 1 where the convergence criteria were set to residual values of $1 \cdot 10^{-6}$.

From figs. 4(a) and 4(b) it could be observed that, there is a significant difference between the results obtained with grids L-1 and M-1, however the values obtained with grids H-1, H-2, and H-3 (not shown) are practically the same, this behavior was observed for all cases. The maximum relative error for all cases between H-1 and H-2 grids was less than 1% for normalized tangential velocity ($U_{tan}/U_{ref}$) and 0.5% for dimensionless temperature, $\theta$.

**Table 1. Grid sensitivity analysis**

| Grid no. | Number of cells | Minimum area [m²] | Maximum area [m²] | $Nu_{avg}$ $L/D = 0.6$ C-0.6 | $Nu_{avg}$ $L/D = 0.6$ S-0.6 |
|---|---|---|---|---|---|
| L-1 | $3.4 \times 10^4$ | $6.3 \times 10^{-4}$ | $5.2 \times 10^{-3}$ | 239.33 | 198.45 |
| M-1 | $6.2 \times 10^4$ | $4.1 \times 10^{-4}$ | $3.1 \times 10^{-3}$ | 242.42 | 199.90 |
| H-1 | $8.9 \times 10^4$ | $3.5 \times 10^{-4}$ | $2.6 \times 10^{-3}$ | 249.71 | 204.88 |
| H-2 | $1.22 \times 10^5$ | $2.9 \times 10^{-4}$ | $2.4 \times 10^{-3}$ | 250.17 | 205.12 |
| H-3 | $1.41 \times 10^5$ | $2.4 \times 10^{-4}$ | $1.9 \times 10^{-3}$ | 250.18 | 205.12 |

### *Model validation*

In order to ensure that the computational model produces physically correct results, comparison with established LDV

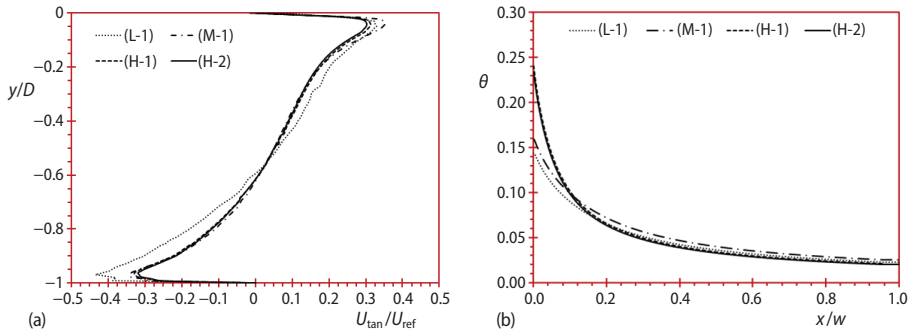


**Figure 4. (a) Predicted normalized tangential velocity, section (a-a) for the three grids case (C-0.2) and (b) predicted dimensionless temperature along adiabatic wall for the three grids case (C-0.2)**

measurements was undertaken. The case sought for validation in the present work is reported in [35]. It represents shear driven flow inside a partially open cylindrical cavity, fixed on the trailing edge of a flat plate. A complete computational analysis of such case has been previously reported by Saqr *et al.* [16]. Figure 5 shows a comparison between numerical results and LDV measurements. The numerical results indicate two turbulence models, showing the prevalence of the standard $k$-$\varepsilon$ model over the $v^2$-$f$ model. The computational model predicted the vortex action resulting from the shear driven flow, however with slight over predictions of velocity in the near wall regions due to the use of the logarithmic law of the wall. The results of the validation case agree well with previous published simulations of turbulent shear driven cavity flows using the $R_e/k$-$\varepsilon$ model for a wide range of Reynolds number [16].

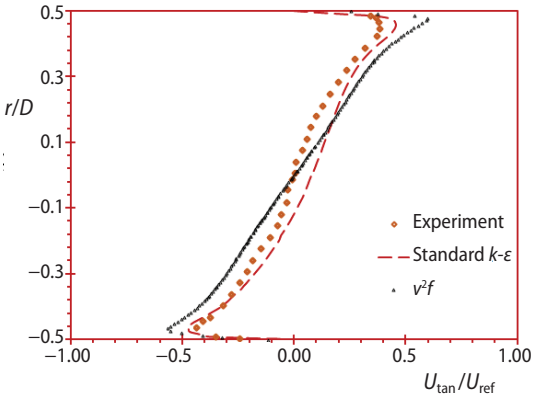


**Figure 5. Comparison of experimental predicted normalized tangential velocity [9, 24] on section (a-a) with two turbulence models, standard $k$-$\varepsilon$, and $v^2$-$f$ for circular cavity, Re = $3 \cdot 10^5$ and Pr = 0.71**

## Results and discussion

Figure 6 shows the profiles of normalized $U_x$ and $U_y$ velocity components as plotted on line (a-a) for square cavity with different opening ratios as given in tab. 2. These profiles show a clear vortex motion occurring in both cavity shapes. In the square cavity, the vortex strength and size are slightly affected by the opening ratio. This is justified by the fact that the size of the square cavity itself is not affected by the change of the opening ratio.

The cavity opening undergoes a shear layer formation leading to enter-mass entrainment between the main flow and the cavity. Figure 7 shows the profiles of normalized $U_y$ velocity component as plotted on (b-b) for both cavity shapes with different opening ratios. Figures 7(a) and 7(b)

**Table 2. Coding the simulation cases for different opening length (L), given as function of the cavity hydraulic diameter (D)**

| Opening ratio | Case | |
|---|---|---|
| | Circular cavity | Square cavity |
| $L/D$ = 1.0 | C-1.0 | S-1.0 |
| $L/D$ = 0.8 | C-0.8 | S-0.8 |
| $L/D$ = 0.6 | C-0.6 | S-0.6 |
| $L/D$ = 0.4 | C-0.4 | S-0.4 |
| $L/D$ = 0.2 | C-0.2 | S-0.2 |

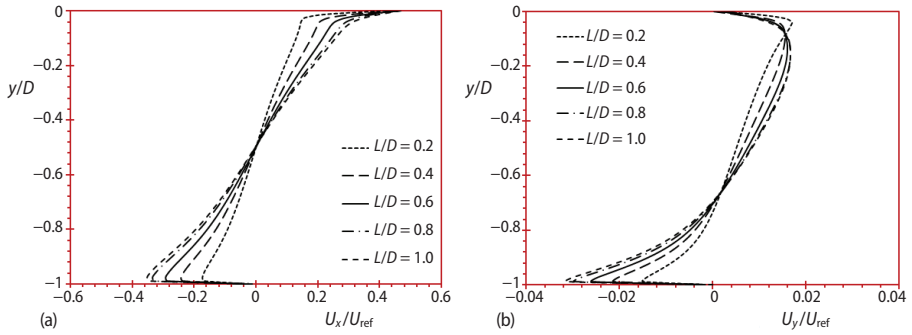


**Figure 6. Normalized velocity components $U_x/U_{ref}$ and $U_y/U_{ref}$ along section (a-a) for square cavity; Re = $3 \cdot 10^5$ and Pr = 0.71**

show that the increase in opening ratio in both cavity shapes corresponds to an increase in $U_y$, which signifies the increase of the enter-mass entrainment. This affects the generation of turbulence in the shear layer, which in turn positively affects the turbulent heat convection within and downstream the cavity.

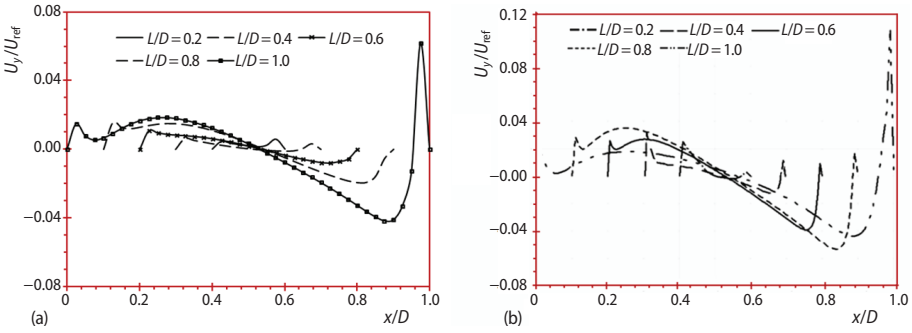


**Figure 7. Normalized y-velocity along section (b-b) for (a) square cavity and (b) circular cavity; Re = $3 \cdot 10^5$ and Pr = 0.71**

The opening ratio was found to affect the turbulence intensity associated with the shear layer formation in the circular cavity, while such effect was insignificant in the square cavity. Figure 8 shows profiles of turbulence intensity on line (b-b) for both cavities at different opening ratios. The turbulence intensity profiles are marked by two locations of maximum value at the separation and reattachment points across the cavity. The nominal value of turbulence intensity increases two to three folds in the square cavity, according to the opening ratio. In the circular cavity, such value increases two to four folds. The increase of turbulence intensity plays a significant role in promoting forced convection within and past the cavity.

Contour-lines of isotherms, $U_x/U_{ref}$, $U_y/U_{ref}$, and vorticity magnitude for circular and rectangular cavities with $L/D$ = 0.2, are presented in fig. 9. The normalized contours of velocity components indicate the vortex symmetry in the circular cavity. This is also indicated by the vorticity contours. In the rectangular cavity, there seems to be more than one vortex. The flow structure in such cavity is characterized by asymmetric vorticity and velocity fields, where the vorticity is intensified in the downstream side of the cavity. The flow complexity of the rectangular cavity implies higher pressure drop than such of the circular cavity, as shown later. It was

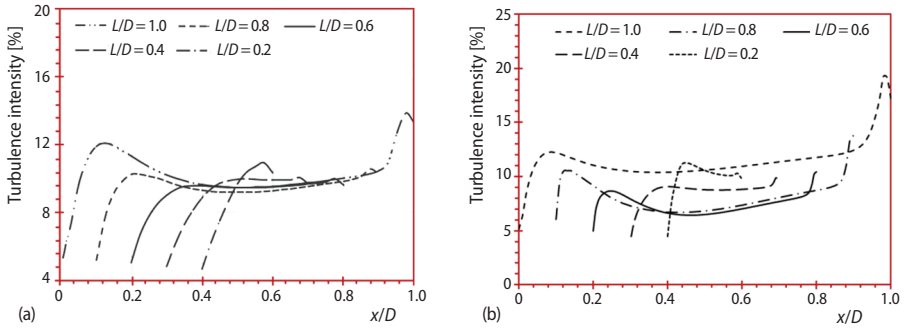


**Figure 8. Turbulence intensity along section (b-b) for (a) square cavity and (b) circular cavity; Re = $3 \cdot 10^5$ and Pr = 0.71**

noted that the utilization of different opening ratios has significant effect on the temperature distribution. The lowest normalized temperature gradient was achieved for opening ratio of 0.6 and 1 for circular and square cavities, respectively, which indicates high local convective heat transfer coefficient across the cavity.

Figures 10(a) and 10(b) demonstrate dimensionless temperature distribution, $\theta$, on downstream surface for different opening ratios. The results show that the cavity shape has a significant effect on the local film cooling performance over the downstream surface. The scheme with circular shape provides the highest film cooling effectiveness at $L/D = 0.6$ among other case studies as shown in fig. 10(b). The scheme with square configuration provides film cooling effectiveness lower than that of the circular at $L/D < 0.4$ and both configurations provide the same performance further downstream at $L/D \geq 0.4$. The scheme with circular configuration provides less boundary-layer thickness over the downstream surface with high velocity. Therefore, the convective heat transfer coefficient was significantly enhanced near the downstream surface.

The quantitative heat transfer results are presented in terms of the local Nusselt number, $\mathrm{Nu}_x$ along the surfaces of the cavity as shown in fig. 11. Starting from the right corner and successively following the bottom, and left edges of the cavity. It can be seen from fig. 11 that the local $\mathrm{Nu}_x$ along the cavity walls have similar behavior with the change of opening ratio for both cavities. The heat exchange was more intense near the left wall next to the opening because of the change in flow direction while exiting the cavity and this resulted in an increase the velocity gradient which in turn enhances the local $\mathrm{Nu}_x$.

In general, the $\mathrm{Nu}_x$ increases with increasing the opening ratio at all surfaces of the cavity. The maximum $\mathrm{Nu}_x$ was achieved at opening ratio of 1 for both circular and square cavities. As stated before, the pressure oscillation in the cavity is a fluid resonant type due to the presence of coupling between the shear layer and the pressure field which in turn affects the turbulent heat convection within and downstream the cavity.

Figure 12(a) shows the effect of the opening ratio and cavity configuration on the average Nusselt number. The circular cavity found to enhance the average Nusselt number over square cavity for all opening ratios, where it increases with the increase of the opening ratio. Equation (14) shows a general formula used in calculation of the average Nusselt number, where, $\Lambda$ is the surface entire length and $\mathrm{Nu}_\lambda$ is the local value of Nusselt number along any direction $\lambda$:

$$\mathrm{Nu} = \frac{1}{\Lambda}\int_0^{\Lambda} \mathrm{Nu}_\lambda \, \mathrm{d}\lambda \tag{14}$$

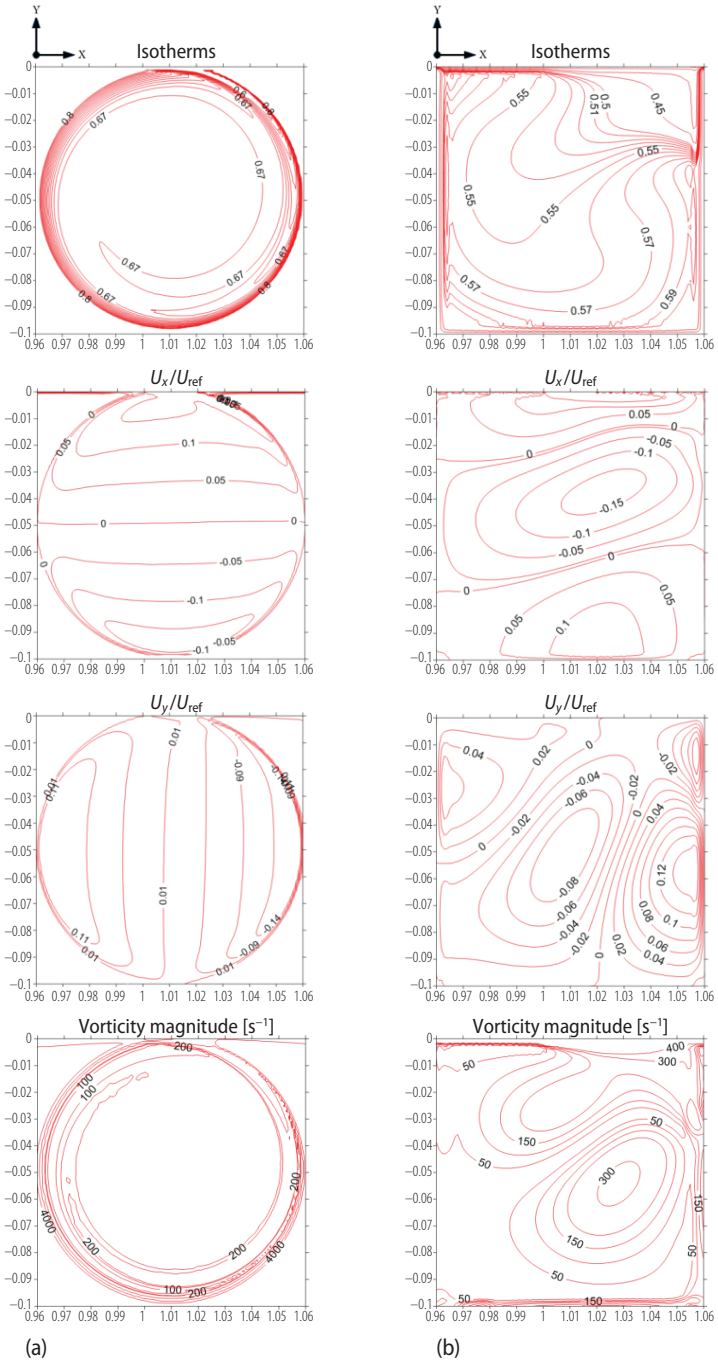


**Figure 9. Normalized dimensionless temperature gradient, $\theta$, normalized x-velocity component, $U_x/U_{ref}$ and normalized y-velocity component $U_y/U_{ref}$ inside (a) partially open circular cavity and (b) partially open square cavity for $L/D = 0.2$, Re = $3 \cdot 10^5$, and Pr = 0.71**

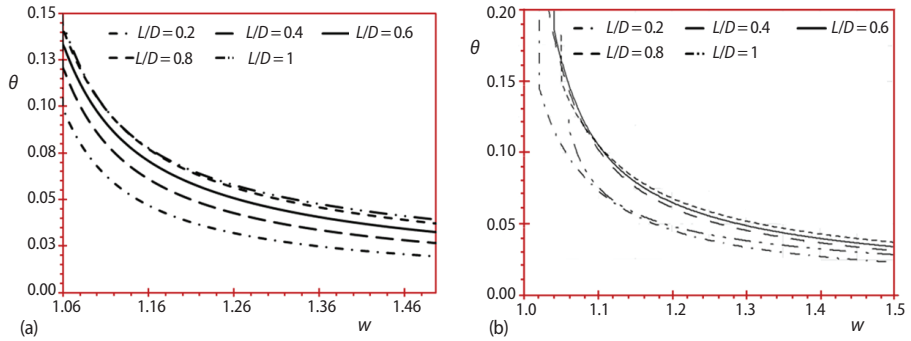


**Figure 10. Normalized dimensionless temperature gradient along adiabatic wall for (a) square cavity and (b) circular cavity; Re = 3·10⁵ and Pr = 0.71**

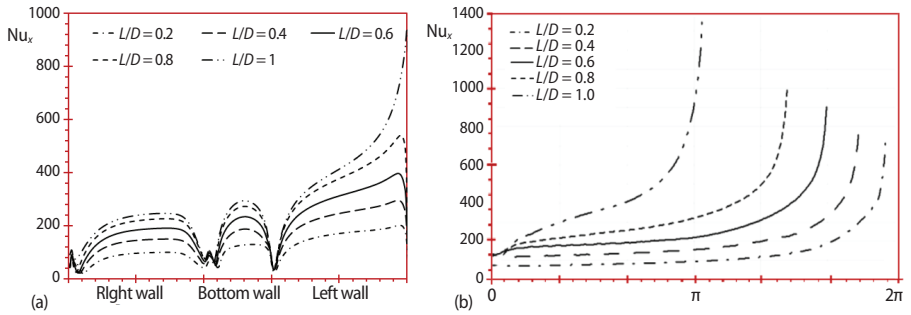


**Figure 11. The $Nu_x$ along cavity walls for (a) square cavity and (b) circular cavity**

The pressure drop, $\Delta P$, across the cavity for circular and square shapes is plotted in figure 12(b). The pressure drop across the cavity was mainly due to the interaction of the shear layer formed over the cavity with the edges of the cavity resulting in pressure feedback phenomenon. Therefore, the pressure field within the cavity was closely coupled with the shear layer formed over the cavity. Both cavity configurations provide a high pressure loss ratio at higher opening ratios. The pressure loss for the circular cavity is approximately one and half times greater than that for the square cavity at $L/D = 1$. This is due to the fact that the shear layer associated with the circular cavity is larger than such associated with the square cavity.

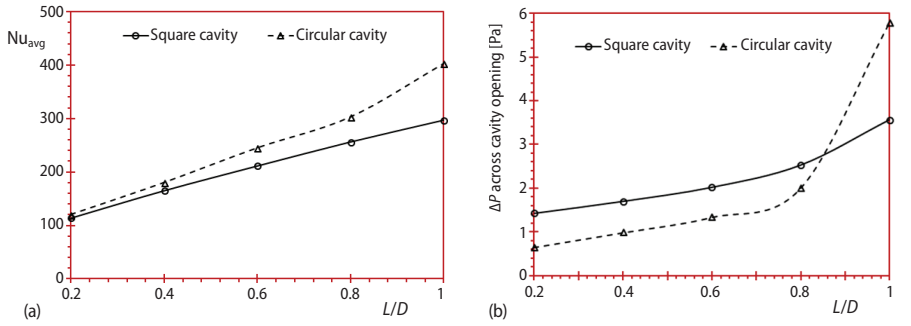


**Figure 12. (a) Average Nusselt number and (b) Pressure drop across cavity openings for different opening ratios, Re = 3·10⁵ and Pr = 0.71**

## Conclusions

The present work introduces the concept of utilizing the shear driven flow in partially open cavities to produce a film cooling effect, where the hot gasses entrain the cavity through the shear layer and then exits to cool the surface downstream the cavity. Numerical simulations for the heat transfer in turbulent flow past a partially open cavity were undertaken to provide a proof of concept for the cooling effect. Different opening ratios were tested in order to find the optimum opening ratio, which achieves the best temperature distribution and minimum pressure drop across the system. Two different cavity geometries were considered: square and circular. The results showed that, thermal and fluid dynamics behavior of the fluid inside the cavity is highly influenced by the opening ratio and the pressure difference across the cavity. When the flow entrained the cavity, large circulations inside the cavity occurred causing an increase in values of local Nusselt number.

Generally, the maximum average Nusselt number was achieved at higher opening ratios for both circular and rectangle cavities. The maximum dimensionless temperature gradient, $\theta$, inside the cavities was achieved at $L/D = 0.2$ for both circular and rectangle cavities. Moreover, for cavities with small opening ratios, small portion of the cooled fluid is exiting the cavity, where larger portion of the fluid is confined within the cavity causing low temperature gradient, $\theta$, downstream the surface. On the other hand, the dimensionless temperature, $\theta$, downstream the cavity reaches its maximum value at opening ratio of 0.6 for circular cavity and 0.8 for rectangle cavity as shown in fig. 10. This is due to that, a large portion of the fluid exits the cavity at lower temperature, but for larger opening ratios a larger portion the fluid exits at higher temperature causing low temperature gradient afterwards.

## Nomenclature

$D$ – cavity hydraulic diameter, [m]
$k$ – turbulent kinetic energy, [m$^2$s$^{-2}$]
$L$ – cavity opening length, [m]
$L/D$ – opening ratio, [–]
Nu – average Nusselt number, [–]
$Nu_x$ – local Nusselt number, [–]
Pr – Prandtl number, [–]
$\Delta P$ – pressure drop, [Pa]
Re – Reynolds number, [–]
$T$ – temperature, [K]
$T_c$ – cold temperature, [K]
$T_h$ – hot temperature, [K]
$U_{ref}$ – reference velocity, [ms$^{-1}$]
$U_{tan}$ – *t*angential velocity, [ms$^{-1}$]
$U_x$ – velocity component in x-direction, [ms$^{-1}$]
$U_y$ – velocity component in y-direction, [ms$^{-1}$]
$w$ – wall length downstream the cavity, [m]

*Greek symbols*

$\varepsilon$ – turbulent dissipation rate, [m$^2$s$^{-3}$]
$\theta$ – dimensionless temperature, [–]

## References

[1] Hossein, N. A. Valizadeh, A. M., A New Approach for the Analysis of the Nanoparticles Effects on Cu-Water Nanofluid Mixed Convection Heat Transfer and Required Power in a Lid-Driven Cavity, *Thermal Science, 20* (2016), 2, pp. 405-414
[2] Pourmahmoud, N., *et al.*, Numerical Study of Mixed Convection Heat Transfer in Lid-Driven Cavity Utilizing Nanofluid: Effect of Type and Model of Nanofluid, *Thermal Science*, *19* (2015), 5, pp. 1575-1590
[3] Madi, A. F., Heat Transfer Prediction in a Shallow Cavity Effect of Incoming Flow Characteristics, *Thermal Science, 20* (2016), 5, pp. 1519-1532
[4] Madi, A. F., *et al.*, Influence of Upstream Flow Characteristics on the Reattachment Phenomenon in Shallow Cavities, *Thermal Science, 15* (2011), 3, pp. 721-734
[5] Mishra, P. D., *et al.*, Numerical Study of Flame/Vortex Interactions in 2-D Trapped Vortex Combustor, *Thermal Science, 18* (2014), 4, pp. 1373-1387
[6] Halouane, Y., *et al.*, Turbulent Heat Transfer for Impinging Jet Flowing Inside a Cylindrical Hot Cavity, *Thermal Science, 19* (2015), 1, pp. 141-154

[7] Shankar, P., Deshpande, M., Fluid Mechanics in the Driven Cavity, *Annual Review of Fluid Mechanics, 32* (2000), Jan., pp. 93-136
[8] Rumyantsev, V. V., Makov, I. P., Energy Losses in Multirow Impingement Cooling of Turbine Blade Leading Edge, *Soviet Aeronautics (English translation of Izvestiya VUZ, Aviatsionnaya Tekhnika), 27* (1984), pp. 41-44
[9] Shuja, S. Z., *et al.*, Local Entropy Generation in an Impinging Jet: Minimum Entropy Concept Evaluating Various Turbulence Models, *Computer Methods in Applied Mechanics and Engineering, 190* (2001), 28, pp. 3623-3644
[10] Shuja, S. Z., *et al.*, Confined Swirling Jet Impingement onto an Adiabatic Wall, *International Journal of Heat and Mass Transfer, 46* (2003), 16, pp. 2947-2955
[11] Shalash, K. M., *et al.*, Numerical Modelling of Slot Film Cooling Using a Wall Function, *Proceedings*, Turbine Technical Conference and Exposition, ASME Turbo Expo, San Antonio, Tex., USA, 2013, Vol. 3B
[12] Mensch, A., Thole, K. A., Overall Effectiveness of a Blade Endwall with Jet Impingement and Film Cooling, *Proceedings*, Turbine Technical Conference and Exposition, ASME Turbo Expo, San Antonio, Tex., USA, 2013, Vol. 3B
[13] Li, X. C., Corder, P., Characteristics of Cooling of the Leading Edge with a Row of Dual Impinging Jets, *Proceedings*, Heat Transfer in Gas Turbines and Jet Engines, ASME, Jacksonville, Fla., USA, 2009, Vol. 2, pp. 625-633
[14] Mhetras, S., *et al.,* Film-Cooling Effectiveness on Squealer Cavity and Rim Walls of Gas-Turbine Blade Tip, *Journal of Propulsion and Power, 22* (2006), 4, pp. 889-899
[15] Syed, S. A., Hoffmann, K. A., Detached Eddy Simulation of Turbulent Flow over a Partially Open Cavity, *Proceedings*, 28th AIAA Applied Aerodynamics Conference, Chicago, Ill., USA, 2010
[16] Saqr, K. M., *et al.*, Computations of Shear Driven Vortex Flow in a Cylindrical Cavity Using a Modified $k$-$\varepsilon$ Turbulence Model, *International Communications in Heat and Mass Transfer, 37* (2010), 8, pp. 1072-1077
[17] Xia, J. L., Zhou, Z. W., Natural Convection in an Externally-Heated Partially-Open Cavity with a Heated Protrusion, *Proceedings*, ASME, Anaheim, Cal., USA, 1992, Vol. 143, pp. 201-208
[18] Bilgen, E., Oztop, H., Natural Convection Heat Transfer in Partially Open Inclined Square Cavities, *International Journal of Heat and Mass Transfer, 48* (2005), 8, pp. 1470-1479
[19] Azzi, A., Jubran, B. A., Numerical Modelling of Film Cooling From Converging Slot-Hole, *Heat and Mass Transfer, 43* (2007), 4, pp. 381-388
[20] Bogard, D., Thole, K., Gas Turbine Film Cooling, *Journal of Propulsion and Power, 22* (2006), 2, pp. 249-270
[21] Liu, C.-L., *et al.*, Film Cooling Performance of Converging Slot-Hole Rows on a Gas Turbine Blade, *International Journal of Heat and Mass Transfer, 53* (2010), 23-24, pp. 5232-5241
[22] Haven, B. A., The Effect of Hole Geometry on the Near Field Character of Crossflow Jets, Accession No. ADA311883, DTIC Document, 1996
[23] Baldauf, S. A., *et al.*, Correlation of Film Cooling Effectiveness from Thermographic Measurements at Engine Like Conditions, *Proceedings*, ASME Turbo Expo 2002: Power for Land, Sea, and Air, American Society of Mechanical Engineers, Amsterdam, The Netherlands, 2002, pp. 149-162
[24] Thole, K., *et al.*, Mean Temperature Measurements of Jets with a Crossflow for Gas Turbine Film Cooling Application, *Proceedings*, 3th International Symposium of Transport Phenomena and Dynamics of Rotating Machinery, Honolulu, Hi, USA, 1990, pp. 69-85
[25] Kadotani, K., Goldstein, R., Effect of Mainstream Variables on Jets Issuing from a Row of Inclined Round Holes, *Journal for Engineering for Power, 101* (1979), 2, pp. 298-304
[26] Leylek, J., Zerkle, R., Discrete-Jet Film Cooling: A Comparison of Computational Results with Experiments, *Journal of Turbomachinery, 116* (1994), 3, pp. 358-368
[27] Ferguson, J. D., *et al.*, Performance of Turbulence Models and Near-Wall Treatments in Discrete Jet Film Cooling Simulations, *Proceedings*, 43rd ASME, International Gas Turbine & Aeroengine Congress & Exhibition, Stockholm, 1998
[28] Lakehal, D., *et al.*, Computation of Film Cooling of a Flat Plate by Lateral Injection From a Row of Holes, *International Journal of Heat and Fluid Flow, 19* (1998), 5, pp. 418-430
[29] Schmitt, F. G., About Boussinesqs Turbulent Viscosity Hypothesis: Historical Remarks and a Direct Evaluation of its Validity, *Comptes Rendus Mecanique, 335* (2007), 9-10, pp. 617-627
[30] Launder, B. E., Spalding, D. B., *Lectures in Mathematical Models of Turbulence*, Academic Press, London, 1972

[31] Launder, B. E., Spalding, D. B., The Numerical Computation of Turbulent Flows, *Computer Methods in Applied Mechanics and Engineering, 3* (1974), 2, pp. 269-289
[32] Durbin, P., Separated Flow Computations with the *k*-epsilon-*v*-squared Model, *AIAA journal, 33* (1995), 4, pp. 659-664
[33] ***, ANSYS, FLUENT 6.3, in, 2006
[34] Launder, B. E. Spalding, D. B., The Numerical Computation of Turbulent Flows, *Computer Methods in Applied Mechanics and Engineering, 3* (1974), 2, pp. 269-289
[35] Savelsberg, R., Castro, I. P., Vortex Flows in Open Cylindrical-Section Cavities, *Experiments in Fluids, 46* (2009), 3, pp. 485-497

Paper submitted: March 9, 2015
Paper revised: June 23, 2015
Paper accepted: July 13, 2015